Fluorescent Sensor Based on Magnetic Separation and Strand Displacement Amplification for the Sensitive Detection of Ochratoxin A

Ruoyu Wu, Jiaping Guo, Minkai Wang, Huimin Liu, Lihua Ding, Ruiying Yang, Li-e Liu,* and Zhiyong Liu*

ACCESS | Metrics & More | Article Recommendations

ABSTRACT: Ochratoxin A (OTA) is a common mycotoxin, and it is a significant threat to human health throughout the food chain. In this study, a sensitive and specific fluorescent sensor based on magnetic separation technology combined with chain displacement amplification was developed for fast and easy detection of OTA in food. The designed strand displacement amplification can improve the sensitivity for the detection, and the magnetic nanomaterials can provide a large surface area, thus enhancing the capture efficiency of the target from the sample. Based on those designs, the experimental results showed that the proposed method displayed excellent performance. The linearity range was 0.5−128.0 ng/mL. The detection limit was 0.125 ng/mL; the relative standard deviations were 3.92−7.71%. Additionally, the developed

method was satisfactorily applied to determine OTA in wheat, corn, and red wine samples at three spiked levels (1.0, 8.0, and 64.0 ng/mL). The recoveries ranged from 85.45 to 107.8% for wheat flour, 101.34 to 108.35% for corn flour, and 91.15 to 93.80% for red wine, respectively. Compared with high-performance liquid chromatography, the proposed method showed a lower limit of detection and equal recovery. Hence, the designed method is a potential and good detecting tool for OTA residue analysis in complex matrix samples.
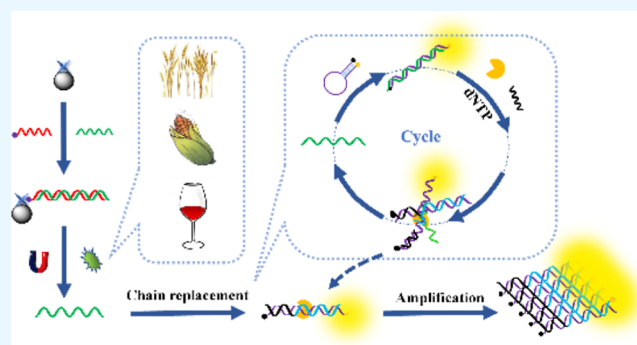
1. INTRODUCTION

Ochratoxins are mycotoxins produced by several certain species of the genera *Aspergillus* and *Penicillium* growing on a wide range of raw food commodities, which mainly include ochratoxin A (OTA), ochratoxin B (OTB), ochratoxin C (OTC), and other structurally similar compounds.[1] OTB and OTC are less toxic and less common than OTA. OTA is produced mainly by *Aspergillus* species, particularly the widespread *Aspergillus ochraceus*. However, in temperate climates, the leading producer is *Penicillium verrucosum*. OTA is the most toxic member of the ochratoxins. OTA is widely found in rice, wheat, corn, coffee, meat, dried fruits, wine,[2] beer, cocoa, nuts, beans, peas,[3] dark teas,[4] milk,[5] and other common foods and their commodities all over the world.[6] OTA can be transferred from contaminated feed to meat, especially pork, and poultry through the food chain. This mycotoxin is structurally similar to the amino acid phenylalanine (Phe). Thus, it has an inhibitory effect on several enzymes that use Phe as a substrate, in particular, Phe-tRNA synthetase, which can result in the inhibition of protein synthesis. It is a mitochondrial poison, causing mitochondrial damage, oxidative burst, lipid peroxidation, and interferes with

oxidative phosphorylation.[7] OTA leads to several types of health risks, including nephrotoxic,[8] hepatotoxic,[9,10] immunosuppressive, genotoxic, carcinogenic,[11] teratogenic, neurotoxic, and mutagenic disease. It is the most crucial form of ochratoxin, categorized as Group 2B of possible human carcinogens by the International Agency for Research on Cancer. In recent years, OTA has been of worldwide concern due to its high toxicity, high chemical stability, and the scope width of contaminated foods and feeds.[12,13] The maximal residue limits of OTA in various foods, feeds, and relevant samples have been officially regulated. Therefore, the detection of OTA in food is of great importance.

In the past decades, thin-layer chromatography[14] has the advantages of low instrumentation requirements, low cost, ease
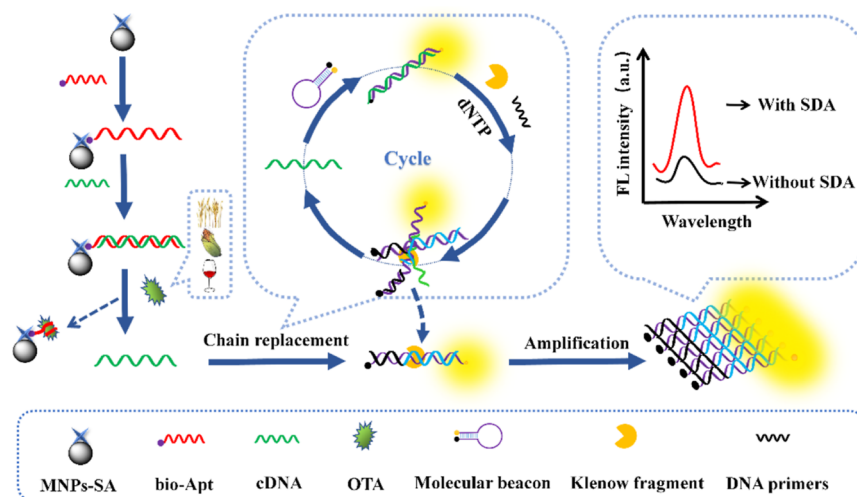
Scheme 1. Fabrication of an FL Aptamer Sensor for OTA Detection

to be popularization, simple operation, and more intuitive results display. However, it also has the disadvantages of requiring more and more complicated reagents, a long detection period, requiring certain technical skills of operators, unsatisfactory reproducibility and sensitivity, difficulty achieving automation, and so forth. In recent years, this method has been gradually replaced by other methods. Other methods, such as high-performance liquid chromatography (HPLC),[15] liquid chromatography-tandem mass spectrometry (LC−MS), and capillary electrophoresis,[16] although highly sensitive, accurate, and stable, usually require more complex and expensive instruments, specialized technicians, and tedious pretreatment steps.[17,18] In addition, enzyme-linked immunosorbent assays and immunochromatographic assays[19] have the advantages of simple operation and rapidity; however, these methods may produce semi-quantitative false-positive results with poor reproducibility. In recent years, photoelectrochemical immunoassay techniques[20,21] have also been widely used in mycotoxin detection. Photoelectrochemical immunoassay technology has the high sensitivity of chemiluminescence assay technology, the high specificity of the immune response, simple instrument construction, simple and rapid analysis method, the optical signal can last a long time, high safety, and long service life of the mycotoxin field detection reflects a great advantage. However, as a short chemiluminescence time, there are substrate interferences, the process requires the use of harmful reagents, harmful to health, and other disadvantages. In summary, the need to establish a rapid, safe, highly sensitive, and highly accurate OTA detection of new methods to meet the actual needs.

Currently, Apt-based sensors have attracted intensive attention as a highly promising OTA sensing and recognition tool. Aptamer (Apt) is typically a short single-stranded oligonucleotide sequence, possessing high-affinity binding and specificity to homologous targets.[22] They are similar to the role of mimic monoclonal antibodies. Compared to antibodies, they display remarkable advantages, such as convenient generation,[23] easy chemical modification, low cost,[24] nontoxicity, little batch-to-batch differences, reversible folding features, non-immunogenicity, high constancy, high sensitive,[25] and reproducibility.[22] These significant features promote the extensive development of aptamer sensors based on electrochemistry,[26,27] photo electrochemistry,[28] and optics,

such as colorimetric methods,[29,30] fluorescence (FL),[31] fluorescent immunity,[32] chemiluminescence,[33,34] surface plasmon resonance,[35] surface-enhanced Raman scattering,[36] and so on. Of these, the sensitivity of the colorimetric method is not high, and the reproducibility of electrochemical and chemiluminescent methods often is not good enough. Meanwhile, the fluorescent aptamer sensor has the advantages of a simple operation process, rapid signal generation, non-destructive operation mode, outstanding sensitivity, good stability and reproducibility, and high throughput detection potential.[37,38] Nowadays, it has been widely used for trace quantitative detection of mycotoxins in food or feed.[39]

Magnetic Fe_3O_4 nanomaterials have the advantages, such as uniform particle size distribution, large specific surface area, strong dispersion, good biological compatibility, easy modification, and significant magnetism, so it is an ideal carrier material with a separation effect.[40] In particular, magnetic separation induces interferences from the complex sample matrix. Therefore, the application of magnetic Fe_3O_4 nanomaterials can significantly improve the sensitivity and selectivity of detection assays.[41]

Common Apt-based FL signal amplification strategies mainly include rolling circle amplification (RCA),[42,43] polymerase chain reaction (PCR),[44] hybridization chain reaction(HCR),[28,45,46] strand displacement amplification (SDA),[47] and so forth comparing with RCA, PCR, and HCR, SDA does not require a specific temperature program to react and is an in vitro isothermal amplification technique. The DNA polymerization reaction of SDA involves the continuous replication of one strand of a DNA double-strand using a polymerase. Meanwhile, the cleavage endonuclease achieves exponential signal amplification by releasing a large amount of ssDNA, which is converted into a readout signal. In addition, polymerization can displace the target from the template when the aptamer sequence is embedded in the SDA template strand, which in turn leads to the next round of recognition reactions and target recovery.[48] It has the advantages of good selectivity, high sensitivity, fast analysis, and real-time detection. It has been widely used for the detection of a variety of targets, such as fungal toxins,[49] nucleic acid molecules,[50] pathogens,[51] thrombin,[52] and adenosine triphosphate.[53]

In this work, a sensitive, specific fluorescent sensor based on magnetic separation coupled with SDA was designed for the detection of OTA. Among them, the aptamers coupled magnetic nanomaterials (MNPs-Apt) were effectively prepared from MNPs-SA and bio-Apt by the high affinity. After that, the complementary strands of DNA (cDNA-1) reacted with the MNPs-Apt, and then, specific MNPs-Apt@cDNA-1 conjugates were obtained. The bio-Apt on the surface of MNPs can precisely identify and capture OTA from the samples. The magnetic nanomaterials can provide a large surface area and thus enhance the capture ability of the OTA. Besides, the SDA, which did not require a specific temperature procedure, was designed to improve the sensitivity of OTA detection. Specifically, it mainly used DNA polymerase with strand replacement function to replace downstream DNA sequences by primer extension, thus achieving the downstream DNA sequence recycling of downstream DNA sequence for product amplification. Therefore, the designed aptamer sensors could be utilized for food safety applications as a practical tool and provide a theoretical basis for establishing and applying other toxin detection techniques.

2. RESULTS AND DISCUSSION

2.1. Principle of a FL Assay. The schematic diagram of the FL aptamer sensor for OTA detection is shown in Scheme 1. First, MNPs-Apt couples were obtained by the specific binding affinity of bio-Apt to streptavidin-coated magnetic beads (MNPs-SA). Next, complementary cDNA-1 was added, and after double-stranded hybridization, cDNA-1 was bound to MNPs-Apt to prepare MNPs-Apt@cDNA-1. When OTA is present, it was bound preferentially to bio-Apt on MNPs-Apt@cDNA-1 by specific affinity action; at the same time, DNA -1 was transferred off MNPs-Apt@cDNA-1 and released into solution. The supernatant was collected by magnetic separation, and the amount of cDNA-1 in the supernatant was positively correlated with OTA. Molecular beacons were then added to the cDNA-1 solution. The high affinity between cDNA-1 and the molecular beacon was used to open the molecular beacon and make its FL. The Klenow fragment, DNA primer, and deoxynucleotide triphosphate (dNTP) were added. Under the action of the Klenow fragment and dNTP, the DNA primer competed down the cDNA-1 and amplified it, generating a FL-emitting DNA primer-molecular beacon-1 complex. The competed cDNA-1 was reused to continue the strand-swap amplification reaction, and the DNA primer-molecular beacon-1 complex was continuously generated, and finally, the amplified FL signal was detected.

2.2. Characterization of MNPs—Apt. The magnetic properties of MNPs-Apt conjugates are shown in Figure 1A. In the natural state, the MNPs-Apt suspension was yellow-brown with good dispersibility. When placed in a magnetic field, the MNPs-Apt rapidly aggregated, and the solution was clear and transparent. The results revealed that the magnetic properties of MNPs-Apt were excellent.

The morphological characteristics of MNPs-Apt can be observed more visually using transmission electron microscopy (TEM). From Figure 1B, it can be seen that MNPs-Apt are nearly spherical, with particle sizes ranging from 150−350 nm. There is no severe adhesion and aggregation.

The size of Zeta potential could be used to judge the stability of nanoparticles in solution. When the absolute value of the zeta potential was 20−30 mV or greater than 30 mV, it represented the medium-stable or high-stable states, respec-
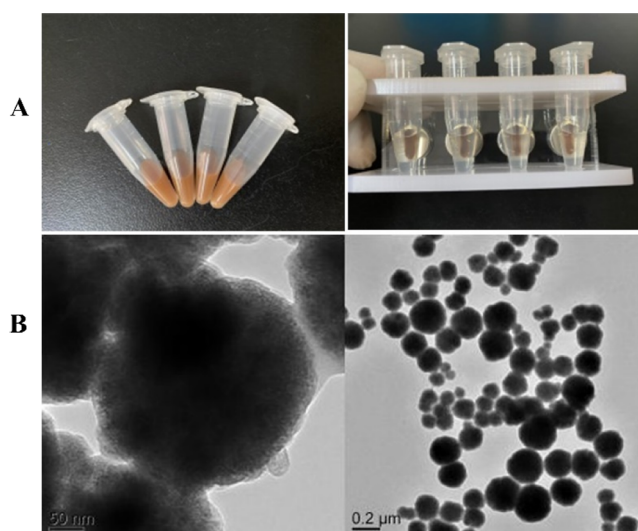

Figure 1. Characteristic of MNPs-Apt. (A) Magnetic characterization of MNPs-Apt, (B) TEM image of MNPs-Apt.

tively.[54] The zeta potential values of MNPs-Apt are shown in Figure 2. It can be seen from the figure that the zeta potential of MNPs-Apt was −21.2 mV, indicating that the suspension of MNPs-Apt was relatively stable and not prone to flocculation.
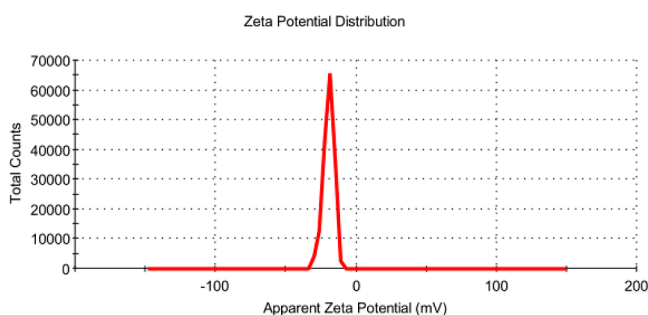

Figure 2. Zeta potential of MNPs-Apt.

In a word, the MNPs-Apt hold good magnetic properties, dispersion, and stability, and it was not easy to aggregate.

2.3. Feasibility of SDA. The results of agarose gel electrophoresis experiments are shown in Figure 3A. It can be seen from the figure that the brightness of lane 3 was stronger than that of lane 2, and its migration distance was smaller than that of lane 2, and it turned out that the molecular beacon and cDNA-1 hybridized successfully. Similarly, lane 4 was similar to that of 3, and the results indicated that molecular beacon, cDNA-1, and primers were successfully hybridized. Besides, the migration distance and brightness of lane 5 were close to lane 2, and its brilliance was significantly lower than that of lanes 3, 4, and 6. From this, in the absence of cDNA-1, the molecular beacon could not hybridize with the primer, and the strand displacement amplification reaction did not occur too. Most importantly, compared to the brightness of the other lanes, the brightness of lane 6 was the strongest. Compared with the situation of lane 4, which was not carried out by the strand displacement amplification, the signal intensity of lane 6, which was performed by the strand displacement amplification, was more remarkable. At the same time, the two strips appeared in lane 6. These phenomena indicated that the strand displacement amplification experiment was successfully de-
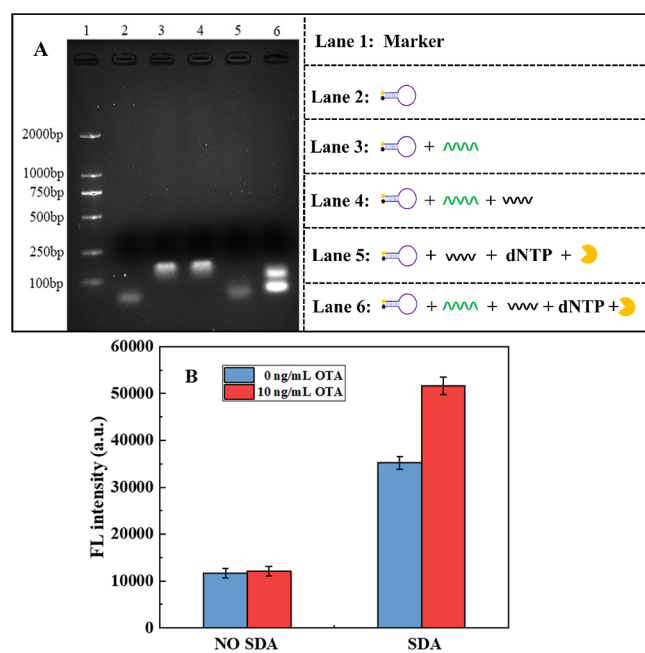
Figure 3. Feasibility analysis. (A) Gel electrophoresis results of strand displacement amplification, (B) comparison of FL signals before and after strand displacement amplification.

signed and could achieve signal amplification. In addition, the two bands in lane 6 suggested that the product was not unique, which had been reported in the literature.[15,55,56]

The effect of SDA technology on sensitivity was further investigated, and the results are shown in Figure 3B. The figure revealed that the FL intensity of the blank solution and the solution of 10 ng/mL OTA did not exceed 12,000 without SDA; while in the SDA system, the FL intensity values of the above solutions were higher, and the FL intensity of the solution of 10 ng/mL OTA was significantly improved. Therefore, SDA effectively enhances the sensitivity of the method. However, the background interference of the SDA system also increased, so it is necessary to optimize the experimental conditions of SDA further.[57−59]

2.4. Performance Optimizations. *2.4.1. Optimization of MNPs-Apt Preparation Conditions.* Under a particular condition, only the dosage of bio-Apt was changed, including 200, 300, 400, 500, and 600 nmol/L, respectively. The effect of the amount of biotinylated OTA aptamers (bio-Apt) on the yield of MNPs-Apt conjugates is shown in Figure 4A. The highest production of MNPs-Apt was observed when the

concentration of biological Apt was 300 nmol/L. Similarly, with other conditions unchanged, only the dosage of MNPs-SA was changed, which was 0.4, 0.7, 1.0, 1.3, and 1.6 mg/mL, respectively. The effect of the amount of MNPs-SA on the yield of MNPs-Apt is shown in Figure 4B. In the range of 0.4−1.3 mg/mL, there was a dose−response relationship. That was, with the increase of the concentration of MNPs-SA, the yield of the conjugate increased. The highest product of MNPs-Apt was obtained when the attention of MNPs-SA was 1.3 mg/mL. When the concentration of MNPs-SA continues to increase, not only will MNPs-SA be wasted, but the excess magnetic beads may also reduce their dispersion and lead to aggregation.[57]

2.4.2. Optimization of Experimental Conditions. In the SDA reaction system, the nucleic acid sequence of cDNA-1 is significant and functions as a "bridge". On the one hand, it directly affected whether it could be competitively displaced from MNPs-Apt@cDNA-1 by OTA and smoothly joined into the process of SDA. On the other hand, when it participated in the process of the SDA, it directly affected whether the hairpin-shaped molecular beacon was smoothly unfolded, and thereby the SDA was well achieved. To this end, three cDNA-1 sequences, such as cDNA-1a, cDNA-1b, and cDNA-1c, were designed by taking the nucleic acid aptamer sequence of OTA as a template. The experimental results showed in Figure 5A that the response value of cDNA-1b was the largest. That is to say, cDNA-1b was an ideal nucleic acid sequence for subsequent experiments.

The MNPs-Apt made by our laboratory was added to the solution containing OTA. The affinity interaction occurred between MNPs-Apt and OTA under certain conditions, and the MNPs-Apt-OTA conjugates were produced. As the reaction progressed, the concentration of OTA in the solution decreased continuously. After the reaction was completed, the magnetic separation was performed, and the FL intensity of the supernatant was measured. The power of the fluorescent signal was positively correlated with the content of OTA. The MNPs-Apt stock solution, the volumes of which were 0, 15, 25, 35, 45, 55, 65, 75, and 85 μL, was added to 50 ng/mL OTA standard solution, respectively. They were mixed well, and the affinity reaction was incubated at 37 °C for 60 min under constant temperature shaking. After that, magnetic separation was performed, the supernatant was taken, and its FL intensity was measured with a FL spectrophotometer. Three copies of each volume. The results are shown in Figure 5B. With the increase of MNPs-Apt, the amount of captured OTA also increased, and there was a dose−effect relationship. When the amount of
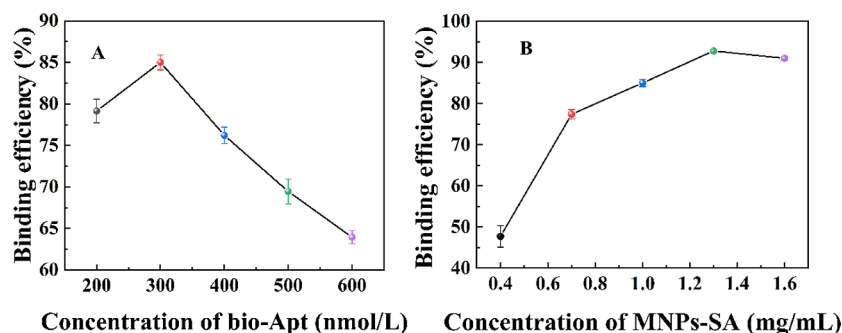

Figure 4. Optimization results of MNPs-Apt preparation conditions. (A) Effects of bio-Apt Concentration on MNPs-Apt binding efficiency; (B) effect of MNPs-SA concentration on MNPs-Apt binding efficiency.
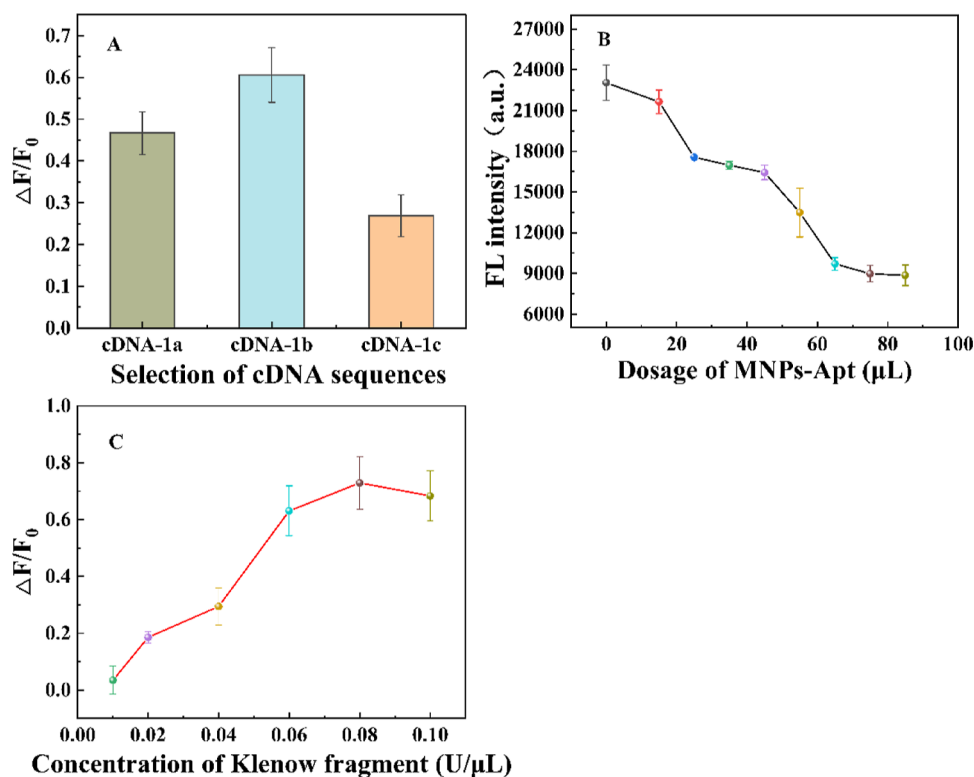
Figure 5. Optimization results of experimental conditions. (A) Optimization of the cDNA-1 base sequence. (B) Influence of MNPS-APT dosage on FL intensity. (C) Influence of Klenow fragment concentration on FL intensity.
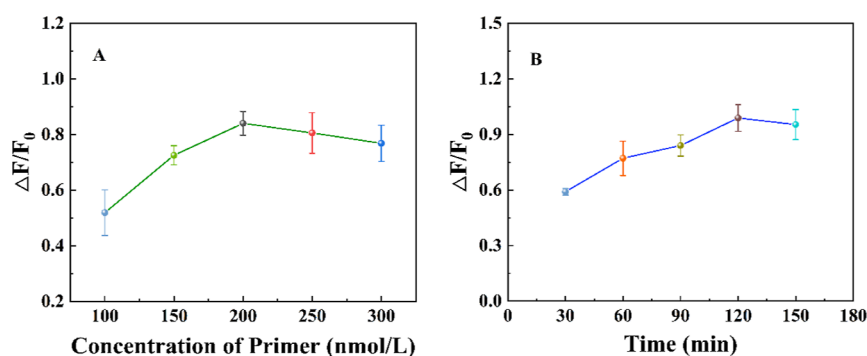

Figure 6. (A) Optimization of primer concentration. (B) Optimization of reaction time for strand displacement amplification.

MNPs-Apt was higher than 65 μL, the FL signal remained unchanged. Therefore, 65 μL was chosen as the optimal amount of MNPs-Apt.

The Klenow fragment is the initiator of the SDA reaction and the key enzyme that determines whether the SDA reaction can proceed. The experiments were carried out under certain conditions, and only the concentrations of the Klenow fragment were changed, which were 0.01, 0.02, 0.04, 0.06, 0.08, and 0.10 U/mL, respectively. The effect of the concentration of the Klenow fragment on SDA is shown in Figure 5C. With the increase of the Klenow fragment, $\Delta F/F_0$ also increased, and there was an apparent dose−effect relationship. When the concentration increased to 0.08 U/μL, the efficiency of the SDA reaction was the highest. Therefore, the optimal concentration of the Klenow fragment was 0.08 U/μL.

The higher the primer concentration, the higher the background of the possible experiment would increase, so

the concentration of the primer was optimized. Experiments were carried out under certain conditions, and only the concentrations of primers were changed, which were 100, 150, 200, 250, and 300 nmol/L, respectively. The effect of primer concentration in SDA is shown in Figure 6A. With the increase of primer concentration, the $\Delta F/F_0$ value first increased and then slowly decreased after reaching a specific deal. When the concentration was at 200 nmol/L, the efficiency of the SDA reaction was the highest.

Finally, the time of strand displacement amplification reaction was investigated. Experiments were done under certain conditions, and only the incubation time of SDA was changed, which were 30, 60, 90, 120, and 150 min, respectively. The effect of reaction time on SDA is shown in Figure 6B. With the prolongation of incubation time, the $\Delta F/F_0$ value first increased and then decreased slightly after reaching a particular value. When the incubation time was 120 min, the efficiency of the SDA reaction was the greatest.
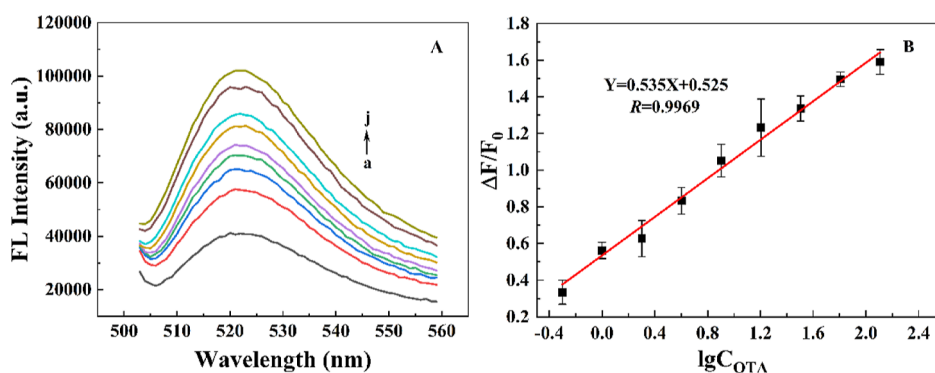
Figure 7. (A) FL intensity of OTA standard solution at different concentrations (curves a–j: 0, 0.5, 1.0, 2.0, 4.0, 8.0, 16.0, 32.0, 64.0, and 128.0 ng/mL). (B) Standard curve of OTA.

2.5. Performance of the Assay System for OTA Measurements.

2.5.1. Calibration Curve and Linear Range.
The calibration curve for OTA was developed under the selected conditions. The results are displayed in Figure 7. The linear range was 0.5−128.0 ng/mL and the calibration curve equation was $\Delta F/F_0 = 0.535 \log C_{OTA} + 0.525$ with a correlation coefficient of 0.9969 (see Figure 7B).

2.5.2. Limit of Detection.
Sensitivity or limit of detection (LOD) was one of the essential indicators to evaluate the detection performance. The LOD was defined as the minimum amount of OTA that can be distinguished from the background signal F_0, and LOD was equal to $\overline{X}_b + 3SD$ ($\overline{X}_b$ and SD was expressed as the mean of the blank sample, and the standard deviation of the blank, respectively). The analytical results showed that LOD was very low at 0.125 ng/mL.

The performance analysis results were also compared with those of other published methods (Table 1). The comparison with other techniques to detect OTA in the last years, the sensitivity and linear range of our method were parallel or superior to the other approaches.

Table 1. Comparison of OTA Detection Strategies

no	method	linear range (ng/mL)	LOD (ng/mL)	refs
1	electrochemical	1−20	0.5	60
2	electrochemical	0.001−1	0.0005	27
3	colorimetric aptamer sensors	8−250	8	61
4	FL	0.5−100	0.07	62
5	FL immunoassays	0.19−1.26	0.12	63
6	FL	4−500	2.0	64
7	immunochromatographic	0.62−5.14	1.79	65
8	FL	0.5−128.0	0.125	this work

2.5.3. Precision.
Three OTA solutions with concentrations of 1.0, 8.0, and 64.0 ng/mL were measured four times to obtain precision. And the accuracy of the method is expressed in terms of relative standard deviation (RSD). The results showed that RSDs were 3.92, 7.71, and 5.97%, respectively.

2.5.4. Selectivity.
Selectivity was another important indicator in evaluating detection performance. According to the calibration curve for FL detection of OTA. 10 ng/mL OTA, 100 ng/mL zearalenone (ZEA), 100 ng/mL aflatoxin B1 (AFB₁), 100 ng/mL OTB, and a mixture of all were analyzed using the established method. The result shows in Figure 8

that the selectivity of the process was good for OTA owing to the precise identification between OTA and bio-Apt.
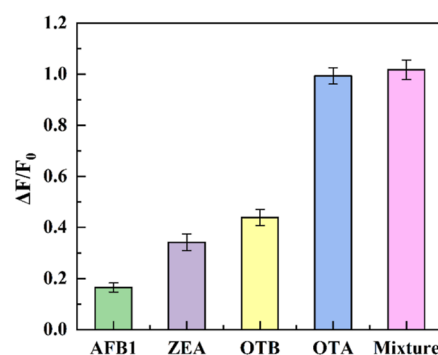

Figure 8. Detection of OTA selectivity.

2.6. Sample Analysis and Accuracy.
To further demonstrate the potential of the proposed practical application, it was used to detect OTA in wheat, corn, and red wine samples prepared as described in Section 4.6. The recovery experiments calculated the accuracy. Each sample was repeated four times, and the average recoveries are reported in Table 2.

2.7. Methods Comparison.
To further demonstrate the potential of this method in practical application, this method was used to conduct sample spike recovery experiments on commercially available wheat flour, corn flour, and red wine. Compared with the popular method HPLC.

For HPLC analysis, conditions were as follows: column, Zorbax Eclipse XDB-C18 (4.6 mm × 250 mm, 5 μm), mobile phase acetonitrile acetic acid (containing 1.11% acetic acid, 42.22% acetonitrile, and 56.67% water v/v/v), flow rate 1.0 mL/min, column temperature 25 °C, and detector 333 nm/460 nm (excitation wavelength/emission wavelength). The calibrants were 5, 10, 20, 50, 100, and 200 ng/mL. A known concentration of OTA (10, 50, and 200 ng/mL) was added to the samples for the recovery test. Then, the calibration curve was $Y = 0.39 + 0.21X$ (Y is the chromatographic peak area, X is the OTA concentration), the linear range was 5−200 ng/mL, and the detection limit was 1.70 ng/mL, and recoveries are given in Table 2.

Compared the developed method with the HPLC method, the results indicated that the detection limit (0.125 ng/mL) was lower than that of HPLC, and the recovery (85.45−107.80% for wheat flour, 101.34−108.35% for corn flour, and 91.15−93.80% for red wine) was equal to that of HPLC. The

Table 2. Recovery Tests for OTA Detection in Real Samples[a]

methods	sample	plus scalar (ng)	measured value (ng)	RSD (%)	recovery rate (%)
aptamer FL	wheat flour	1	0.85 ± 0.13	15.12	85.45
		8	8.62 ± 1.02	11.86	107.80
		64	56.72 ± 7.02	12.37	88.62
	corn flour	1	1.01 ± 0.06	6.23	101.34
		8	8.39 ± 1.24	14.76	104.92
		64	58.53 ± 10.28	17.57	108.35
	red wine	1	0.91 ± 0.01	0.98	91.30
		8	7.29 ± 0.53	7.31	91.15
		64	60.03 ± 3.60	5.99	93.80
HPLC	wheat flour	10	9.49 ± 0.33	3.45	94.86
		50	49.49 ± 0.73	1.48	98.99
		200	195.22 ± 5.14	2.63	97.61
	corn flour	10	9.55 ± 0.29	3.05	95.55
		50	47.62 ± 3.24	6.80	95.23
		200	188.66 ± 18.32	9.71	94.33
	red wine	10	9.07 ± 0.72	7.95	90.66
		50	48.35 ± 2.60	5.37	96.70
		200	184.80 ± 8.45	4.57	92.40

[a]Note: OTA was not detected from the three samples.

Table 3. DNA Oligonucleotide Sequences Used in This Work

oligonucleotide name	sequence (from 5′ to 3′) description
aptamer	biotin-AAAAAAAAAAAAGATCGGGTGTGGGTGGCGTAAAGGGAGCATCGGACA
cDNA-1a	TTACGCCACCCACACCCGATC
cDNA-1b	CCTTTACGCCACCCACACCCGATC
cDNA-1c	CGCCACCCACACCCGATC
molecular beacon	FAM-TCTTGGAGATCGGGTGTGGGTGGCGTAAAGGGTCCAAGA-Dabcy
DNA primer	TCTTGGAC

proposed method's precision was not as good as that of HPLC, but it could meet the needs of quantitative analysis.

3. CONCLUSIONS

A highly sensitive, specific method based on strand displacement amplification technique and magnetic separation has been developed to measure OTA. The MNPs-Apt obtained by reacting bio-Apt with MNPs-SA has solid magnetic properties, stability, and high specificity. The strand displacement amplification reaction achieved signal magnification and improved the sensitivity in the developed method. Additionally, the application in the real spiked food or beverage samples confirmed the dependability and integrity of the proposed method. Compared with HPLC, the built method held a better analytical performance with a lower detection limit. However, the current experimental steps are numerous and can be considered to simplify the experimental steps by integrating the complementary DNA strand and nucleic acid aptamer into a single strand to construct a nucleic acid aptamer of the departure clamp type. Overall, the method can be used as a potentially better detection tool for OTA analysis in real samples of complex matrices. It can also show the underlying application prospects in the food safety field.

4. MATERIALS AND METHODS

4.1. Chemicals and Solutions. Analytical standards for OTA, ZEA, AFB1, and OTB were purchased from Pribolab (Qingdao, China). A 2000 bp DNA ladder was obtained from CWBIO (Beijing, China). The Klenow fragment was purchased from Takara (Beijing, China). The nucleic acids

were provided by Sangon Biotech (Shanghai) Co., Ltd. The nucleic acid names and base sequences are shown in Table 3. Phosphate-buffered saline (PBS) buffer dry powder, TE buffer solution (pH of 8.0), Tween20, Tris, and dNTPs mixture were bought from Beijing Solarbio (Beijing, China).

The solutions used in this experiment were as follows. The nucleic acids were dissolved in TE (Tris and EDTA) buffer solution. Then, it was placed on the PCR instrument and heated at 95 °C for 5 min. After that, it was cooled to room temperature. Subsequently, the processed nucleic acids were stored in a refrigerator at 4 °C for later use. The incubation solution was 0.01 mol/L of sodium PBS, pH of 7.4. Another buffer solution was composed of 10 mmol/L Tris, 20 mmol/L $CaCl_2$, 5 mmol/L KCl, 20 mmol/L NaCl, and 20 mmol/L $MgCl_2 \cdot 6H_2O$, pH of 8.5. The electrophoresis buffer solution (50× TAE) consisted of 242 g of Tris, 37.2 g of EDTA, and 57.1 mL of glacial acetic acid, whose volume was 1000 mL. The electrophoresis buffer solution (1× TAE) was prepared by diluting the stored, concentrated solution with ultrapure water. The OTA standard solutions were obtained by serial dilutions of the standard solution (25 μg/mL) with the buffer solution (pH of 8.5), and their respective concentrations were 0.5, 1.0, 2.0, 4.0, 8.0, 16.0, 32.0, 64.0, and 128.0 ng/mL, respectively. The experimental water was ultrapure (resistivity ≥ 18.2 MΩ· cm at 25 °C).

4.2. Instrumentation and Parameters. The MNPs-SA with the size of 300 nm was provided by BioMag Scientific (2 mg/mL. Wuxi, China). The FL signal was measured by an FS5 FL spectrophotometer (Edinburgh Instruments, UK). A Nanodrop 2000 ultrafine ultraviolet spectrophotometer

(Thermo Fisher Scientific) was used to identify the nucleic acid aptamers' reaction. A Zeta sizer Nano-ZS 90 (laser particle size and zeta potential analyzer, Malvern, UK) was applied to explore the hydrodynamic diameter and zeta potential of MNPs-Apt conjugates, which were prepared from bio-Apt with MNPs-SA by particular affinity. In addition, A JEM2100 transmission electron microscope (Japan) was used to depict the morphology characterization of the conjugates. An electrophoresis apparatus was applied to perform the electrophoresis experiment to ensure the smooth progress of the strand displacement amplification reaction. Another instrument used in this paper for comparative analysis was HP 1100 HPLC (Agilent Technologies, USA).

4.3. Preparation of MNPs-Apt Conjugates. 300 μL of 1 mg/mL MNPs-SA was added into a 1.5 mL low-adsorption EP tube. The MNPs-SA were washed with PBS buffer solution and magnetically separated. It was washed with PBS buffer solution three times. After that, 300 μL of 400 nmol/L bio-Apt PBS buffer solution (referred to as pre) was taken to the MNPs-SA suspension, mixed well, and incubated at 37 °C for 30 min with constant temperature shaking. After the reaction, MNPs-Apt conjugates were gained, magnetic separation was performed, and the supernatant was taken, referred to as post. Finally, the above conjugates were washed with 300 μL of PBS buffer, and the washing was repeated twice, and the supernatants were denoted as wash1 and wash2, respectively. The optical density of the supernatant solutions of pre, post, wash1, and wash2 was measured with an ultra-micro-UV spectrophotometer at a wavelength of 260 nm, and the coupling efficiency was calculated according to formula 1. Subsequently, the MNPs-Apt. conjugates were suspended in the buffer solution (pH of 8.5). Finally, the conjugates were stored at 4 °C for use.

$$\text{binding efficiency}(\%)$$
$$= \frac{\text{OD}_{260(\text{pre})} - \text{OD}_{260(\text{post})} - \text{OD}_{260(\text{wash1})} - \text{OD}_{260(\text{wash2})}}{\text{OD}_{260(\text{pre})}}$$
$$\times 100\% \tag{1}$$

4.4. Agarose Gel Electrophoresis of SDA. Detection in the OTA system, to ensure that SDA is performed properly, the agarose gel electrophoresis experiments were used to examine it. First, 0.80 g of agarose was added to a clean conical flask, and 40 μL 1× TAE electrophoresis buffer solution was also combined in the bottle. Then, it was shaken well and heated until transparent in a microwave. It was poured into the electrophoresis tank. After that, 4 μL Gold view I nucleic acid dye was slowly poured into the electrophoresis tank, cooled, and set aside. Next, the electrophoresis tank was put into the electrophoresis device, and a 1× TAE electrophoresis buffer solution was added to this tank. The height of the buffer solution was slightly higher than the height of the gel. The Marker standard solution was added directly to the wells of lane 1. Another 10 μL of the sample was thoroughly blended with 2 μL of loading buffer and added to other wells in the gel. Finally, the power supply of the electrophoresis apparatus was turned on, and the electrophoresis voltage and time were set at 100 V and 30 min, respectively. Furthermore, the gel imaging of the standard Marker and samples was revealed on a gel imager.

4.5. Procedure for OTA Detection. 65 μL of MNPs-Apt conjugates was thoroughly mixed with 35 μL of cDNA-1 and

incubated at 37 °C for 30 min in a shaker. The MNPs-Apt@ cDNA-1 complex was obtained by the chain hybridization reaction, and separated by a magnetic effect, while the fluid was discarded. Then, a 20 μL of OTA calibrant or food sample was added to the MNPs-Apt@cDNA-1 complex solution and incubated at 37 °C for 60 min under shaking. Magnetic separation was performed, and the cDNA-1 substituted by OTA competition was obtained in the supernatant solution. After that, 20 μL of molecular beacon solution was added to the above cDNA-1 solution and reacted at 37 °C for 30 min under constant temperature shaking. Finally, 10 μL of DNA primers, 8.8 μL of dNTP mixed solution, and 1.2 μL of 4.0 U/ μL Klenow fragment solution were sequentially added to the above solution (cDNA-1+molecular beacon), mixed thoroughly, and the displacement amplification reaction was carried out at 37 °C for 120 min in a constant temperature shaker. After that, the FL intensity at 519 nm was detected by the FS5 FL spectrophotometer.

4.6. Detection of the Food Samples. The wheat flour, corn flour, and red wine samples were all purchased from the local market. The wheat and corn samples were pretreated as described in the literature,[66] and the red wine sample was prepared according to ref.[67] An approximate 2.5 g of the cereal sample was mixed with 10 mL of methanol. Then, the upper mixture was homogenized for 3 min at high speed. It was performed for 30 min at 180 W power on an ultrasonic instrument. After ultrasonic and centrifugal separation, the supernatant solution was filtrated with a 0.22 μm organic needle filter for further use. The red wine solution was diluted appropriately with the PBS buffer. Each sample was spiked with known amounts of OTA standard solution at 1.00, 8.00, and 64.00 ng/mL concentrations and then detected as described above for OTA by the proposed method.

■ AUTHOR INFORMATION

Corresponding Authors

Li-e Liu − *College of Public Health, Zhengzhou University, Zhengzhou 450001, People's Republic of China;* orcid.org/0000-0001-6770-9944; Phone: +86 371 67781246; Email: zzdxlle66@126.com; Fax: +86 371 67781919

Zhiyong Liu − *Key Laboratory of Food Safety Quick Testing and Smart Supervision Technology for State Market Regulation, Beijing 100094, People's Republic of China;* Email: liuzhiyong9@126.com

Authors

Ruoyu Wu − *College of Public Health, Zhengzhou University, Zhengzhou 450001, People's Republic of China*

Jiaping Guo − *College of Public Health, Zhengzhou University, Zhengzhou 450001, People's Republic of China*

Minkai Wang − *Department of Neurosurgery, First Affiliated Hospital of Zhengzhou University, Zhengzhou, Henan 450052, People's Republic of China*

Huimin Liu − *College of Public Health, Zhengzhou University, Zhengzhou 450001, People's Republic of China*

Lihua Ding − *College of Public Health, Zhengzhou University, Zhengzhou 450001, People's Republic of China*

Ruiying Yang − *College of Public Health, Zhengzhou University, Zhengzhou 450001, People's Republic of China*

Complete contact information is available at:
https://pubs.acs.org/10.1021/acsomega.3c01408

Notes

The authors declare no competing financial interest.

■ REFERENCES

(1) Bennett, J. W.; Klich, M. Mycotoxins. *Clin. Microbiol. Rev.* **2003**, *16*, 497−516.

(2) Liu, Y.; Liu, D.; Cui, S.; Li, C.; Yun, Z.; Zhang, J.; Sun, F. Design of a Signal-Amplified Aptamer-Based Lateral Flow Test Strip for the Rapid Detection of Ochratoxin A in Red Wine. *Foods* **2022**, *11*, 1598.

(3) Acuña-Gutiérrez, C.; Jiménez, V. M.; Müller, J. Occurrence of mycotoxins in pulses. *Compr. Rev. Food Sci. Food Saf.* **2022**, *21*, 4002−4017.

(4) Zhang, X.; Zhang, L.; Zhou, T.; Zhou, Y. Fungal flora and mycotoxin contamination in tea: Current status, detection methods and dietary risk assessment - A comprehensive review. *Trends Food Sci. Technol.* **2022**, *127*, 207−220.

(5) Sun, J.; Li, M.; Xing, F.; Wang, H.; Zhang, Y.; Sun, X. Novel dual immunochromatographic test strip based on double antibodies and biotin-streptavidin system for simultaneous sensitive detection of aflatoxin M1 and ochratoxin A in milk. *Food Chem.* **2022**, *375*, 131682.

(6) Ganesan, A. R.; Mohan, K.; Karthick Rajan, D.; Pillay, A. A.; Palanisami, T.; Sathishkumar, P.; Conterno, L. Distribution, toxicity, interactive effects, and detection of ochratoxin and deoxynivalenol in food: A review. *Food Chem.* **2022**, *378*, 131978.

(7) Marin, S.; Ramos, A. J.; Cano-Sancho, G.; Sanchis, V. Mycotoxins: occurrence, toxicology, and exposure assessment. *Food Chem. Toxicol.* **2013**, *60*, 218−237.

(8) Zhao, T.; Shen, X. L.; Chen, W.; Liao, X.; Yang, J.; Wang, Y.; Zou, Y.; Fang, C. Advances in research of nephrotoxicity and toxic antagonism of ochratoxin A. *Toxin Rev.* **2016**, *36*, 39−44.

(9) Chae, S. A.; Pyo, M. C.; Yoo, H. J.; Lee, K.-W. Ochratoxin a induces hepatic fibrosis through TGF-β receptor I/Smad2/3 signaling pathway. *Environ. Toxicol.* **2022**, *37*, 2084−2095.

(10) Pfohl-Leszkowicz, A.; Manderville, R. A.; Ochratoxin, A. Ochratoxin A: An overview on toxicity and carcinogenicity in animals and humans. *Mol. Nutr. Food Res.* **2007**, *51*, 61−99.

(11) Heussner, A. H.; Bingle, L. E. H. Comparative Ochratoxin Toxicity: A Review of the Available Data. *Toxins* **2015**, *7*, 4253−4282.

(12) Kebede, H.; Liu, X.; Jin, J.; Xing, F. Current status of major mycotoxins contamination in food and feed in Africa. *Food Control* **2020**, *110*, 106975.

(13) Haque, A.; Wang, Y.; Shen, Z.; Li, X.; Saleemi, M. K.; He, C. Mycotoxin contamination and control strategy in human, domestic animal and poultry: A review. *Microb. Pathog.* **2020**, *142*, 104095.

(14) Rocha, D. F. d.L.; Oliveira, M. D. S.; Furlong, E. B.; Junges, A.; Paroul, N.; Valduga, E.; Backes, G. T.; Zeni, J.; Cansian, R. L. Evaluation of the TLC quantification method and occurrence of deoxynivalenol in wheat flour of southern Brazil. *Food Addit. Contam., Part A* **2017**, *34*, 2220−2229.

(15) Andrade, M. A.; Lancas, F. M. Determination of Ochratoxin A in wine by packed in-tube solid phase microextraction followed by high performance liquid chromatography coupled to tandem mass spectrometry. *J. Chromatogr., A* **2017**, *1493*, 41−48.

(16) Cheng, Z.; Choi, N.; Wang, R.; Lee, S.; Moon, K. C.; Yoon, S.-Y.; Chen, L.; Choo, J. Simultaneous Detection of Dual Prostate Specific Antigens Using Surface-Enhanced Raman Scattering-Based Immunoassay for Accurate Diagnosis of Prostate Cancer. *ACS Nano* **2017**, *11*, 4926−4933.

(17) Suea-Ngam, A.; Howes, P. D.; Stanley, C. E.; deMello, A. J. An Exonuclease I-Assisted Silver-Metallized Electrochemical Aptasensor for Ochratoxin A Detection. *ACS Sens.* **2019**, *4*, 1560−1568.

(18) Jiang, C.; Lan, L.; Yao, Y.; Zhao, F.; Ping, J. Recent progress in application of nanomaterial-enabled biosensors for ochratoxin A detection. *Trends Anal. Chem.* **2018**, *102*, 236−249.

(19) Zhang, Y.; Wang, L.; Shen, X.; Wei, X.; Huang, X.; Liu, Y.; Sun, X.; Wang, Z.; Sun, Y.; Xu, Z.; Eremin, S. A.; Lei, H. Broad-Specificity Immunoassay for Simultaneous Detection of Ochratoxins A, B, and C in Millet and Maize. *J. Agric. Food Chem.* **2017**, *65*, 4830−4838.

(20) Lin, Y.; Zhou, Q.; Tang, D.; Niessner, R.; Yang, H.; Knopp, D. Silver Nanolabels-Assisted Ion-Exchange Reaction with CdTe Quantum Dots Mediated Exciton Trapping for Signal-On Photo-electrochemical Immunoassay of Mycotoxins. *Anal. Chem.* **2016**, *88*, 7858−7866.

(21) Lin, Y.; Zhou, Q.; Tang, D. Dopamine-Loaded Liposomes for in-Situ Amplified Photoelectrochemical Immunoassay of AFB(1) to Enhance Photocurrent of Mn(2+)-Doped Zn(3)(OH)(2)V(2)O(7) Nanobelts. *Anal. Chem.* **2017**, *89*, 11803−11810.

(22) Qiu, Z.; Shu, J.; Liu, J.; Tang, D. Dual-Channel Photo-electrochemical Ratiometric Aptasensor with up-Converting Nano-crystals Using Spatial-Resolved Technique on Homemade 3D Printed Device. *Anal. Chem.* **2018**, *91*, 1260−1268.

(23) An, K.; Lu, X.; Wang, C.; Qian, J.; Chen, Q.; Hao, N.; Wang, K. Porous Gold Nanocages: High Atom Utilization for Thiolated Aptamer Immobilization to Well Balance the Simplicity, Sensitivity, and Cost of Disposable Aptasensors. *Anal. Chem.* **2019**, *91*, 8660−8666.

(24) Qiu, Z.; Shu, J.; Tang, D. Bioresponsive Release System for Visual Fluorescence Detection of Carcinoembryonic Antigen from Mesoporous Silica Nanocontainers Mediated Optical Color on Quantum Dot-Enzyme-Impregnated Paper. *Anal. Chem.* **2017**, *89*, 5152−5160.

(25) Lv, S.; Zhang, K.; Zhu, L.; Tang, D. ZIF-8-Assisted NaYF4:Yb,Tm@ZnO Converter with Exonuclease III-Powered DNA Walker for Near-Infrared Light Responsive Biosensor. *Anal. Chem.* **2020**, *92*, 1470−1476.

(26) Wang, Y.; Ning, G.; Wu, Y.; Wu, S.; Zeng, B.; Liu, G.; He, X.; Wang, K. Facile combination of beta-cyclodextrin host-guest recognition with exonuclease-assistant signal amplification for sensitive electrochemical assay of ochratoxin A. *Biosens. Bioelectron.* **2019**, *124−125*, 82−88.

(27) Wang, X.; Shan, Y.; Gong, M.; Jin, X.; Lv, l.; Jiang, M.; Xu, J. A novel electrochemical sensor for ochratoxin A based on the hairpin aptamer and double report DNA via multiple signal amplification strategy. *Sens. Actuators, B* **2019**, *281*, 595−601.

(28) Zhao, Y.; Xiang, J.; Cheng, H.; Liu, X.; Li, F. Flexible photoelectrochemical biosensor for ultrasensitive microRNA detection based on concatenated multiplex signal amplification. *Biosens. Bioelectron.* **2021**, *194*, 113581.

(29) Lin, C.; Zheng, H.; Sun, M.; Guo, Y.; Luo, F.; Guo, L.; Qiu, B.; Lin, Z.; Chen, G. Highly sensitive colorimetric aptasensor for ochratoxin A detection based on enzyme-encapsulated liposome. *Anal. Chim. Acta* **2018**, *1002*, 90−96.

(30) Yu, X.; Lin, Y.; Wang, X.; Xu, L.; Wang, Z.; Fu, F. Exonuclease-assisted multicolor aptasensor for visual detection of ochratoxin A based on G-quadruplex-hemin DNAzyme-mediated etching of gold nanorod. *Microchim. Acta* **2018**, *185*, 259.

(31) Feng, J.; Qian, Y.; Cheng, Q.; Ma, Y.; Wu, D.; Ma, H.; Ren, X.; Wang, X.; Wei, Q. A signal amplification of p DNA@Ag2S based photoelectrochemical competitive sensor for the sensitive detection of OTA in microfluidic devices. *Biosens. Bioelectron.* **2020**, *168*, 112503.

(32) Guo, X.; Wang, M.; Ma, L.; Cui, Z.; Liu, Z.; Yang, H.; Liu, Y. Carboxyl porphyrin as signal molecule for sensitive fluorescent detection of aflatoxin B(1) via ARGET-ATRP. *Spectrochim. Acta, Part A* **2022**, *280*, 121535.

(33) Li, Y.; Sun, L.; Zhao, Q. Aptamer-Structure Switch Coupled with Horseradish Peroxidase Labeling on a Microplate for the

Sensitive Detection of Small Molecules. *Anal. Chem.* **2019**, *91*, 2615−2619.

(34) Shen, P.; Li, W.; Liu, Y.; Ding, Z.; Deng, Y.; Zhu, X.; Jin, Y.; Li, Y.; Li, J.; Zheng, T. High-Throughput Low-Background G-Quadruplex Aptamer Chemiluminescence Assay for Ochratoxin A Using a Single Photonic Crystal Microsphere. *Anal. Chem.* **2017**, *89*, 11862−11868.

(35) Zhang, Z. H.; Lei, K. N.; Li, C. N.; Luo, Y. H.; Jiang, Z. L. A new and facile nanosilver SPR colored method for ultratrace arsenic based on aptamer regulation of Au-doped carbon dot catalytic amplification. *Spectrochim. Acta, Part A* **2020**, *232*, 118174.

(36) Liu, M.; Li, X.; Li, B.; Du, J.; Yang, Z. A fluorometric aptamer-based assay for ochratoxin A by using exonuclease III-assisted recycling amplification. *Mikrochim. Acta* **2019**, *187*, 46.

(37) Zhu, S.; Wang, S.; Xia, M.; Wang, B.; Huang, Y.; Zhang, D.; Zhang, X.; Wang, G. Intracellular Imaging of Glutathione with MnO(2) Nanosheet@Ru(bpy)(3)(2+)-UiO-66 Nanocomposites. *ACS Appl. Mater. Interfaces* **2019**, *11*, 31693−31699.

(38) Chen, J.; Han, T.; Feng, X.; Wang, B.; Wang, G. A poly(thymine)-templated fluorescent copper nanoparticle hydrogel-based visual and portable strategy for an organophosphorus pesticide assay. *Analyst* **2019**, *144*, 2423−2429.

(39) Kim, K.; Jo, E.-J.; Lee, K. J.; Park, J.; Jung, G. Y.; Shin, Y.-B.; Lee, L. P.; Kim, M.-G. Gold nanocap-supported upconversion nanoparticles for fabrication of a solid-phase aptasensor to detect ochratoxin A. *Biosens. Bioelectron.* **2020**, *150*, 111885.

(40) Hou, Y.; Jia, B.; Sheng, P.; Liao, X.; Shi, L.; Fang, L.; Zhou, L.; Kong, W. Aptasensors for mycotoxins in foods: Recent advances and future trends. *Compr. Rev. Food Sci. Food Saf.* **2021**, *21*, 2032−2073.

(41) Chen, X.; Gao, D.; Sun, F.; Li, Z.; Wang, Y.; Qiu, C.; He, K.; Wang, J. Nanomaterial-based aptamer biosensors for ochratoxin A detection: a review. *Anal. Bioanal. Chem.* **2022**, *414*, 2953−2969.

(42) Yang, L.; Zhang, Y.; Li, R.; Lin, C.; Guo, L.; Qiu, B.; Lin, Z.; Chen, G. Electrochemiluminescence biosensor for ultrasensitive determination of ochratoxin A in corn samples based on aptamer and hyperbranched rolling circle amplification. *Biosens. Bioelectron.* **2015**, *70*, 268−274.

(43) Jiang, S.; Liu, M.; Tantai, W.; Xu, Q.; Zou, X.; Ma, F.; Zhang, C.-Y. Aptamer-mediated rolling circle amplification for label-free and sensitive detection of histone acetyltransferase activity. *Chem. Commun.* **2021**, *57*, 2041−2044.

(44) Qing, Y.; Li, X.; Chen, S.; Zhou, X.; Luo, M.; Xu, X.; Li, C.; Qiu, J. Differential pulse voltammetric ochratoxin A assay based on the use of an aptamer and hybridization chain reaction. *Microchim. Acta* **2017**, *184*, 863−870.

(45) Gu, C.; Kong, X.; Liu, X.; Gai, P.; Li, F. Enzymatic Biofuel-Cell-Based Self-Powered Biosensor Integrated with DNA Amplification Strategy for Ultrasensitive Detection of Single-Nucleotide Polymorphism. *Anal. Chem.* **2019**, *91*, 8697−8704.

(46) Yang, L.; Yin, X.; An, B.; Li, F. Precise Capture and Direct Quantification of Tumor Exosomes via a Highly Efficient Dual-Aptamer Recognition-Assisted Ratiometric Immobilization-Free Electrochemical Strategy. *Anal. Chem.* **2021**, *93*, 1709−1716.

(47) Chang, J.; Lv, W.; Wu, J.; Li, H.; Li, F. Simultaneous photoelectrochemical detection of dual microRNAs by capturing CdS quantum dots and methylene blue based on target-initiated strand displaced amplification. *Chin. Chem. Lett.* **2021**, *32*, 775−778.

(48) Cai, R.; Yin, F.; Zhang, Z.; Tian, Y.; Zhou, N. Functional chimera aptamer and molecular beacon based fluorescent detection of Staphylococcus aureus with strand displacement-target recycling amplification. *Anal. Chim. Acta* **2019**, *1075*, 128−136.

(49) Yin, J.; Liu, Y.; Wang, S.; Deng, J.; Lin, X.; Gao, J. Engineering a universal and label-free evaluation method for mycotoxins detection based on strand displacement amplification and G-quadruplex signal amplification. *Sens. Actuators, B* **2018**, *256*, 573−579.

(50) Deng, X.; Wang, C.; Gao, Y.; Li, J.; Wen, W.; Zhang, X.; Wang, S. Applying strand displacement amplification to quantum dots-based fluorescent lateral flow assay strips for HIV-DNA detection. *Biosens. Bioelectron.* **2018**, *105*, 211−217.

(51) Wu, W.; Zhao, S.; Mao, Y.; Fang, Z.; Lu, X.; Zeng, L. A sensitive lateral flow biosensor for Escherichia coli O157:H7 detection based on aptamer mediated strand displacement amplification. *Anal. Chim. Acta* **2015**, *861*, 62−68.

(52) Huang, Z.; Luo, Z.; Chen, J.; Xu, Y.; Duan, Y. A Facile, Label-Free, and Universal Biosensor Platform Based on Target-Induced Graphene Oxide Constrained DNA Dissociation Coupling with Improved Strand Displacement Amplification. *ACS Sens.* **2018**, *3*, 2423−2431.

(53) Wang, Y.-M.; Liu, J.-W.; Duan, L.-Y.; Liu, S.-J.; Jiang, J.-H. Aptamer-based fluorometric determination of ATP by using target-cycling strand displacement amplification and copper nanoclusters. *Microchim. Acta* **2017**, *184*, 4183−4188.

(54) Khalesi, M. Ochratoxin A in liquorice products - a review. *Food Addit. Contam., Part A: Chem., Anal., Control, Exposure Risk Assess.* **2015**, *32*, 1−7.

(55) Santos Pereira, C.; C Cunha, S.; Fernandes, J. O. Prevalent Mycotoxins in Animal Feed: Occurrence and Analytical Methods. *Toxins* **2019**, *11*, 290.

(56) Li, M.; Tong, Z.; Gao, X.; Zhang, L.; Li, S. Simultaneous detection of zearalenone, citrinin, and ochratoxin A in pepper by capillary zone electrophoresis. *Food Addit. Contam., Part A: Chem., Anal., Control, Exposure Risk Assess.* **2020**, *37*, 1388−1398.

(57) Rocha, D. F. d. L.; Oliveira, M. D. S.; Furlong, E. B.; Junges, A.; Paroul, N.; Valduga, E.; Backes, G. T.; Zeni, J.; Cansian, R. L. Evaluation of the TLC quantification method and occurrence of deoxynivalenol in wheat flour of southern Brazil. *Food Addit. Contam., Part A: Chem., Anal., Control, Exposure Risk Assess.* **2017**, *34*, 2220−2229.

(58) Zhang, X.; Chen, L.; Li, J.; Zhu, B.; Ma, L. Occurrence of Ochratoxin A in Chinese wines: influence of local meteorological parameters. *Eur. Food Res. Technol.* **2012**, *236*, 277−283.

(59) De Jesus, C. L.; Bartley, A.; Welch, A. Z.; Berry, J. P. High Incidence and Levels of Ochratoxin A in Wines Sourced from the United States. *Toxins* **2017**, *10*, 1.

(60) Radi, A. E.; Munoz-Berbel, X.; Lates, V.; Marty, J. L. Label-free impedimetric immunosensor for sensitive detection of ochratoxin A. *Biosens. Bioelectron.* **2009**, *24*, 1888−1892.

(61) Yang, C.; Wang, Y.; Marty, J. L.; Yang, X. Aptamer-based colorimetric biosensing of Ochratoxin A using unmodified gold nanoparticles indicator. *Biosens. Bioelectron.* **2011**, *26*, 2724−2727.

(62) He, Y.; Yu, Y.; Wen, X.; Shi, Y.; Wu, J.; Guan, Z.; Cui, M.; Xiao, C. A quencher-free 2-aminopurine modified hairpin aptasensor for ultrasensitive detection of Ochratoxin A. *Spectrochim. Acta, Part A* **2020**, *228*, 117780.

(63) Wang, X.; Wang, Y.; Wang, Y.; Chen, Q.; Liu, X. Nanobody-alkaline phosphatase fusion-mediated phosphate-triggered fluorescence immunoassay for ochratoxin a detection. *Spectrochim. Acta, Part A* **2020**, *226*, 117617.

(64) Ma, Q.; Nie, D.; Sun, X.; Xu, Y.; He, J.; Yang, L.; Yang, L. A versatile Y shaped DNA nanostructure for simple, rapid and one-step detection of mycotoxins. *Spectrochim. Acta, Part A* **2022**, *281*, 121634.

(65) Hu, X.; Zhang, G. An Immunochromatographic Test Strip to Detect Ochratoxin A and Zearalenone Simultaneously. *Methods Mol. Biol* **2017**, *1600*, 95−105.

(66) Aswani Kumar, Y. V. V.; Renuka, R. M.; Achuth, A. J.; Mudili, V.; Poda, S.; Mudili, V.; Poda, S. Development of a FRET-based fluorescence aptasensor for the detection of aflatoxin B1 in contaminated food grain samples. *RSC Adv.* **2018**, *8*, 10465−10473.

(67) Samokhvalov, A. V.; Safenkova, I. V.; Eremin, S. A.; Zherdev, A. V.; Dzantiev, B. B. Use of anchor protein modules in fluorescence polarisation aptamer assay for ochratoxin A determination. *Anal. Chim. Acta* **2017**, *962*, 80−87.